The effect of doping amount of Zn on the co-evaporated SnSe thin film for photovoltaic application

FEI ZHAO[1,*], JUNHAO CHU[2]
[1]*School of Photoelectric Engineering, Changzhou Institute of Technology, Changzhou, Jiangsu, 213002, China*
[2]*Shanghai Institute of Technical Physics, Chinese Academy of Sciences, Shanghai 200083, China*

In this work, SnSe thin films were prepared by co-evaporation method with different Zn doping amount, and the comparative studies were carried out. Experimental results indicate that the SnSe thin film with 0.285% Zn doping amount possesses higher electron mobility (32.69 $cm^2V^{-1}s^{-1}$), lower resistivity (1.32 Ωcm), better crystalline, larger grain size, which promotes the efficiency improvement of the SnSe thin film solar cell. The efficiency of the SnSe device is improved to 0.55% by Zn doping. These results guide better growth of SnSe thin film and contribute to the development of the SnSe thin film solar cell.

(Received August 10, 2021; accepted June 7, 2022)

Keywords: Zn doping, Co-evaporation, SnSe thin film, Solar cell

1. Introduction

In recent decades, many researchers have made great attempts to solve the problem of energy consumption that has caused a lot of distress. Through unremitting efforts, many renewable energy sources have been discovered, supplying an important solution to rapidly growing energy requirements. Solar energy is inexhaustible. Utilizing solar energy makes the development of new energy conversion materials and compounds become an important direction for future research [1-4]. Solar cells with absorption layer materials such as CIGS and CdTe have been deeply studied and respectively obtained high conversion efficiency of 23.35% and 22.1% [5]. Although their efficiencies are greatly improved, the toxicity of In, Ga and Cd hinder their further research [6]. Thus, finding new light absorbing materials is an advisable way. SnSe thin films with good optical and electrical properties attract widespread attention in practical applications, such as in solar cells [7, 8], infrared (IR) detector [9] and lithium ion battery electrodes [10]. SnSe is particularly important in photovoltaic applications due to the theoretical maximum power conversion efficiency of 32%. Besides, SnSe is relatively non-toxic and earth-rich [11-13].

In order to improve the performance of SnSe and SnSe-based compounds, some researchers have studied the effects of substitution, high temperature, doping, high pressure, and strain on their electronic, magnetic, and thermoelectric properties [14-20]. Some researchers have also studied the high carrier mobility of the SnSe magnitude under biaxial strain [21-22]. However, few people study the effect of doping on the light absorption enhancement performance of SnSe. There are many methods for the synthesis of SnSe, including: chemical bath deposition [23], electrodeposition [24], thermal evaporation [25], and chemical vapor deposition (CVD) [26]. Considering the cost and complexity of material synthesis, vacuum method is very important. Besides, the substrate temperature, evaporation rate, and film thickness are easily controlled during the deposition of SnSe thin film. In this study, the vacuum method was used to achieve the synthesis of metal tin compounds. This method makes the surface morphology and the ratio of each element of the film depend on the substrate temperature, evaporation rate, and purity of the material. In addition, since many of the physical properties of SnSe thin films are highly shape-dependent, shape-controlled, synthesis of doped and undoped structures is a huge challenge. Many studies have

controlled the bandgap energy of chalcognide nanostructures by doping different materials (such as SnS, PbS, ZnTe, etc.) to change its electrical and optical properties [27-30]. The study finds that metal dopants can enhance the physical properties of the thin film, such as increasing electron mobility and decreasing resistivity, which exhibit great significance in enhancing the optical performance of solar cells.

According to the reports we have read, no researchers study the effect of the doping amount of Zn on the optical properties of SnSe. Hence, we enhanced the microstructure, optical and electrical properties of SnSe thin film by changing the doping amount of Zn. Finally, SnSe solar cells were fabricated and a best power conversion efficiency of 0.55% was achieved.

2. Experimental

2.1. Deposition of thin films

SnSe thin films were prepared by co-evaporation on bare glass substrate and molybdenum coated soda lime glass substrate using Sn (purity of 99.999%), Se (purity of 99.999%) and Zn (purity of 99.999%) as raw materials. In order to analyze the effects of doping amount of Zn on the properties of SnSe thin films, the doping amount of Zn was controlled to 0%, 0.285%, 0.501%, 0.823% and 0.978% respectively. About 1μm Zn-doped SnSe thin film was synthesized on bare glass substrate and molybdenum coated soda lime glass substrate by co-evaporation method. To control the same evaporated environment during sample preparation, all the Zn-doped SnSe thin films were carried on a vacuum environment and the system operating pressure is 10^{-5} Torr. Besides, the substrate temperature was controlled to 500 ℃. The Zn-doped SnSe thin films prepared on molybdenum coated soda lime glass substrate were integrated into the solar cell, and the Zn-doped SnSe absorbers prepared on bare glass substrate was used for optical characteristics, electrical characteristics, structural analysis and surface morphology analysis. A 80 nm CdS buffer layer was deposited on the top of the prepared SnSe absorber film with rf-sputtering method at room temperature for 5 min, deposition power for 100 W and in 0.5 Pa pure Ar atmosphere, followed by depositing a 80 nm i-ZnO layer and a 1500 nm ITO layer. The i-ZnO layer was deposited by rf-sputtering process using an intrinsic ZnO target at room temperature for 5 min, deposition power for 90 W and in 0.6 Pa pure Ar. The ITO layer was deposited by rf-sputtering process using an ITO target at room temperature for 14 min, deposition power for 100 W and in 0.6 Pa pure Ar. Nickel (60 nm) and aluminum (400 nm) top contacts were obtained by electron beam evaporation deposition. No etching, element doping, diffusion barrier or anti-reflection coating were used in the device fabrication in this work and the total area of each Zn-doped SnSe solar cell is about 0.42 cm^2. The structure of Zn-doped SnSe solar cell in this work are shown in Fig. 1.

Fig. 1. The structure of Zn-doped SnSe thin film solar cell (color online)

2.2. Characterizations

The Raman spectra was measured by Raman spectrometer (Jobin–Yvon T64000). The structure was taken by X-ray diffraction (XRD, Rigaku D/max 2550 V) with Cu Ka radiation. The doping amount of Zn was estimated by X-ray fluorescence analysis (XRF, SHIMADZU EDX-7000). The optical parameters were taken by Cary5000 UV–VIS–NIR spectrophotometer. The surface morphology was achieved by scanning electron microscopy (SEM, JEOL). The electrical properties of the films were determined by Hall Effect measurement (Ecopia, HMS3000). The current-voltage (J-V) characteristic was achieved by a solar simulator (Newport Xe-lamp) with a source meter (Keithley 2400) at 100 mW/cm^2, AM1.5 G illumination.

3. Results and discussions

3.1. Optical properties

Table 1 shows the elemental composition of the films, which was measured by X-ray fluorescence analysis (XRF, SHIMADZU EDX-7000). The optic transmittance reflects the absorption coefficient, and the absorption coefficient reflects the band gap energy, which makes optic transmittance very important in semiconductors. It can be concluded from the optic transmittance that the forbidden band width of a semiconductor is mainly due to the fact that the value of the transmittance will suddenly decrease near the transmission spectrum due to the conversion between frequency bands, which can enable this material to be practically applied in different devices. The optical properties of the prepared Zn-doped and undoped SnSe thin film were studied using Cary5000 UV–VIS–NIR spectrophotometer. From the results of the study, it was found that the transmittance of the SnSe thin films varied with the doping amount of Zn. For photons of wavelength between 400 and 1400 nm, a transmittance of 0.01-24% is obtained. As shown in Fig. 2, for photons with a wavelength of 400-1400 nm, the undoped SnSe thin film obtains the highest transmission of 0.01-24%, and a 0.285% Zn-doped SnSe thin film obtains the lowest of 0.01-5.60% transmittance. This is because as the doping amount of Zn changes, the strain value changes in the SnSe layer close to the glass substrate. We use the transmittance data to calculate the absorption coefficient and optical band gap. The absorption coefficient (a) can be obtained from the transmittance and Equation (1),

$$\alpha = \frac{1}{\mathrm{d}}\ln(\frac{1}{T}) \quad (1)$$

where d is the path length, T is the transmittance of the SnSe thin film, and a is the absorption coefficient. The band gap of SnSe can be obtained by Equation (2),

$$(\mathrm{ahv})^n = A\ (\mathrm{hv} - E_g) \quad (2)$$

where the value of E_g is depending on the type of band transition of the material. The band gap obtained when n is 1/2 is the indirect band gap (Davis-Mott model) and the band gap obtained when n is 2 is the direct band gap (Tauc's model) [31-32]. Fig. 3a shows the relationship between the Tauc's curve $(ahv)^2$ and the photon energy hv for determining the direct band gap, and Fig. 3b shows the Davis-Mott curve showing the relationship between $(ahv)^{1/2}$ and the photon energy hv to determine the indirect Bandgap. Fig. 3a shows that the value of the direct band gap E_g of SnSe is between 0.9 and 1.1 eV and the value of the indirect band gap E_g of SnSe observed from Fig. 3b is between 0.86 and 0.98 eV. The changes of direct and indirect band gap is due to the difference in stacking faults and lattice defects as the changes of doping amount of Zn. The obtained direct and indirect band gap values are comparable to those given by Singh [33], which is consistent with theoretical expectations. The results obtained in this work are in good agreement with earlier reports of SnSe thin films prepared by other method [34]. When considering the relationship between band gap energy and solar cell efficiency, it can be seen that all SnSe thin films obtained are suitable for photovoltaic applications.

Table 1. Elemental composition of the films

S. No.	Sn (at.%)	Se (at.%)	Zn (at.%)
1	51.782	48.218	0
2	50.072	49.643	0.285
3	50.382	49.117	0.501
4	49.354	49.823	0.823
5	50.060	48.962	0.978

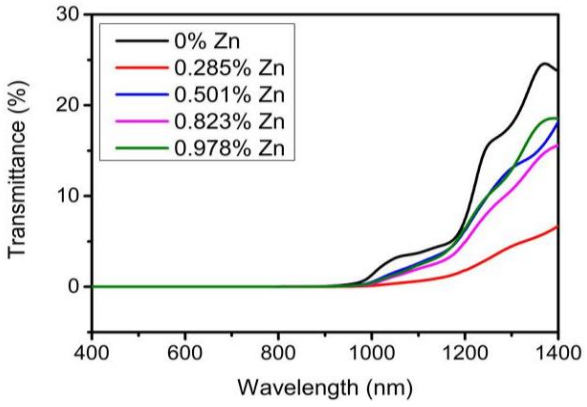

Fig. 2. Transmittance of SnSe thin films with different doping amount of Zn (color online)

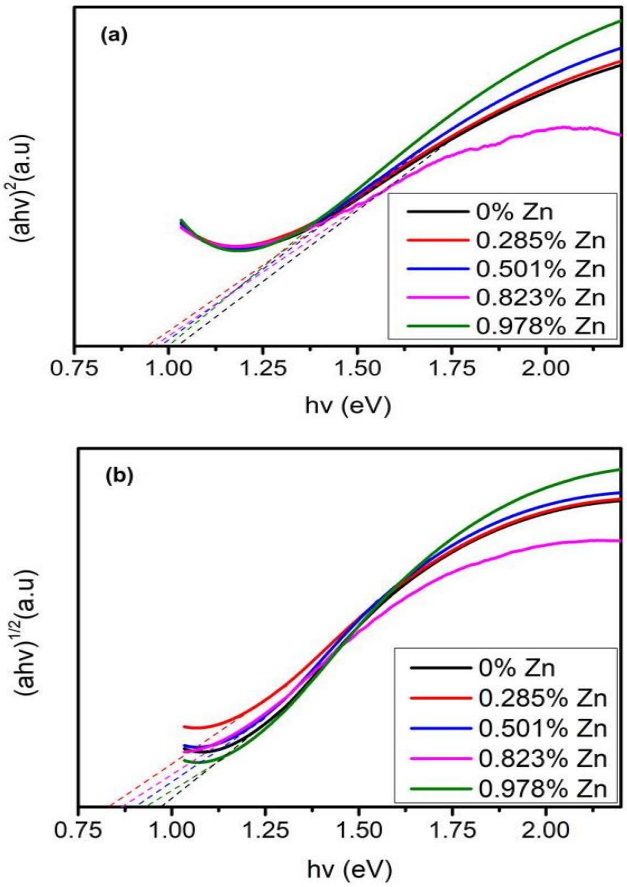

Fig. 3. (a) Direct band gap and (b) indirect band gap of SnSe thin films with different doping amount of Zn (color online)

The optical properties of SnSe thin films were further analyzed by Raman spectroscopy. The excitation wavelength of the Raman spectrum is 542 nm, and the measurement range is 50 to 300 cm^{-1}. Fig. 4 shows the Raman spectra of the prepared Zn-doped and undoped SnSe. It can be seen that all the Raman spectrum show four vibration modes at 74 cm^{-1}, 105.8 cm^{-1}, 130 cm^{-1}, and 152 cm^{-1} and these vibration modes correspond to A^1g, B_{3g}, A^2g and A^3g modes respectively [35-36], which conform to the characteristic pattern of SnSe well. Ag and B_{3g} are two rigid shear modes of the layer relative to its adjacent layers, they determine the characteristic planar vibration modes of orthorhombic phase SnSe.

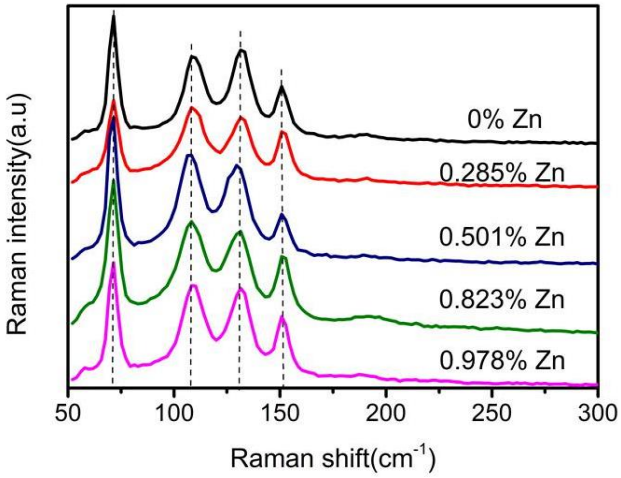

Fig. 4. Raman spectra of SnSe thin films with different doping amount of Zn (color online)

3.2. Crystalline structure

The X-ray diffraction data of undoped SnSe and Zn-doped samples are shown in the Fig. 5(a). All diffraction peaks can be indexed to the phase of SnSe (Standard Identification Card, JCPDS 48-1224), belonging to the orthorhombic structure without impurity peaks. Fig. 5(b) shows the magnified XRD patterns and demonstrates the peak deviation at (111) and (400). Comparing the XRD results of those pellets, it is clear that the (111) peak of 0.285% Zn-doped SnSe is much stronger than that of pure SnSe and others, and the (400) peak of 0.501% Zn-doped SnSe is also stronger than that of pure SnSe and others. The occurrence of the (111) peak and (400) peak helps to improve the efficiency of the solar cell [37]. The high intensity peak of (111) shifted towards a higher angle as the Zn content increased in the samples, which resulted from the difference in effective ionic radius based on the Bragg relation ($n\lambda = 2d\sin\theta$). According to lower ionic radius of Zn (0.88 Å) compared with Sn (0.93 Å), it is expected a decrease in d-spacing (the distance between the crystalline planes) of Zn-doped SnSe films.

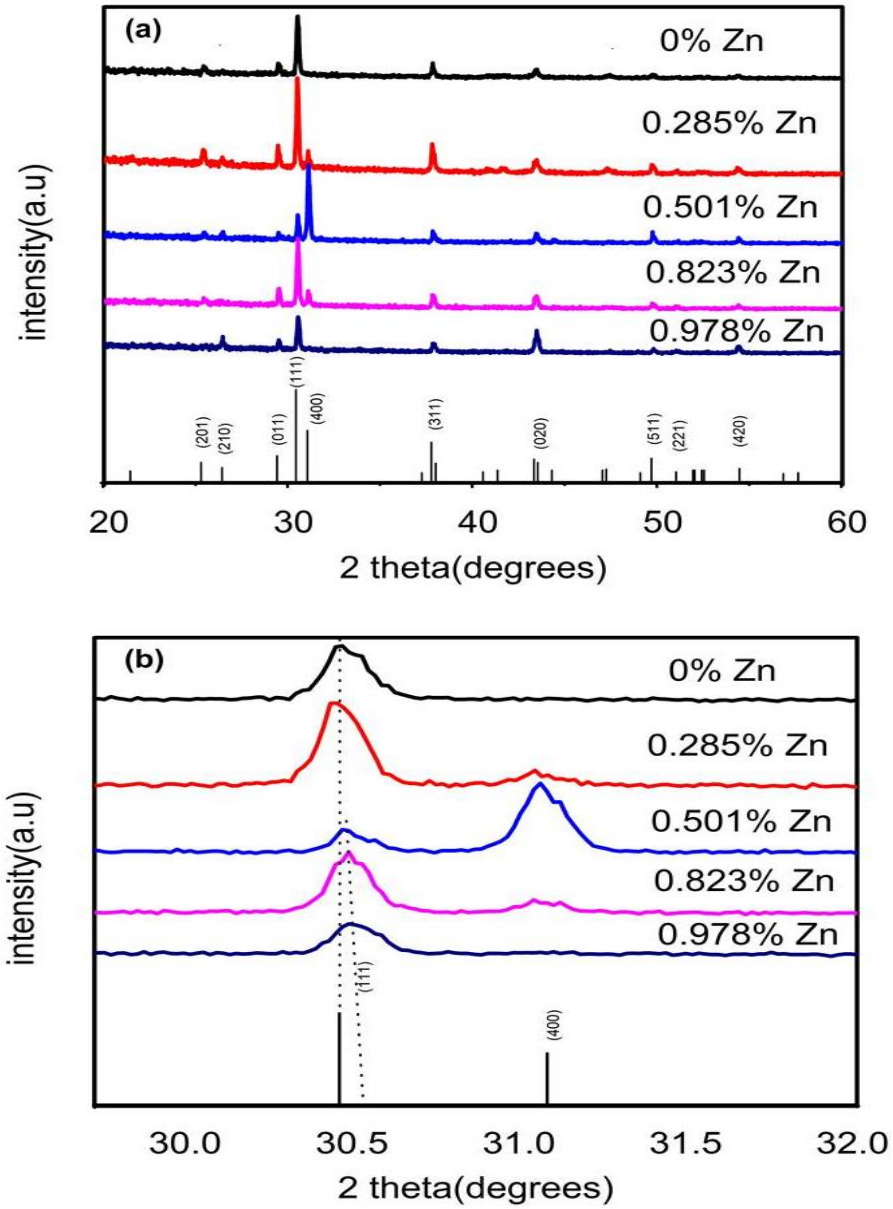

Fig. 5. (a) XRD patterns and (b) detailed XRD patterns near 30.51° of SnSe thin films with different doping amount of Zn (color online)

3.3. Morphological characterization

Fig. 6 shows the surface SEM images of undoped and Zn-doped SnSe thin films. Although the microcrystals for all SnSe thin films are dense and uniformly distributed over the film surface, the microstructure (shape and grain size) of the samples depends on the doping amount of Zn.

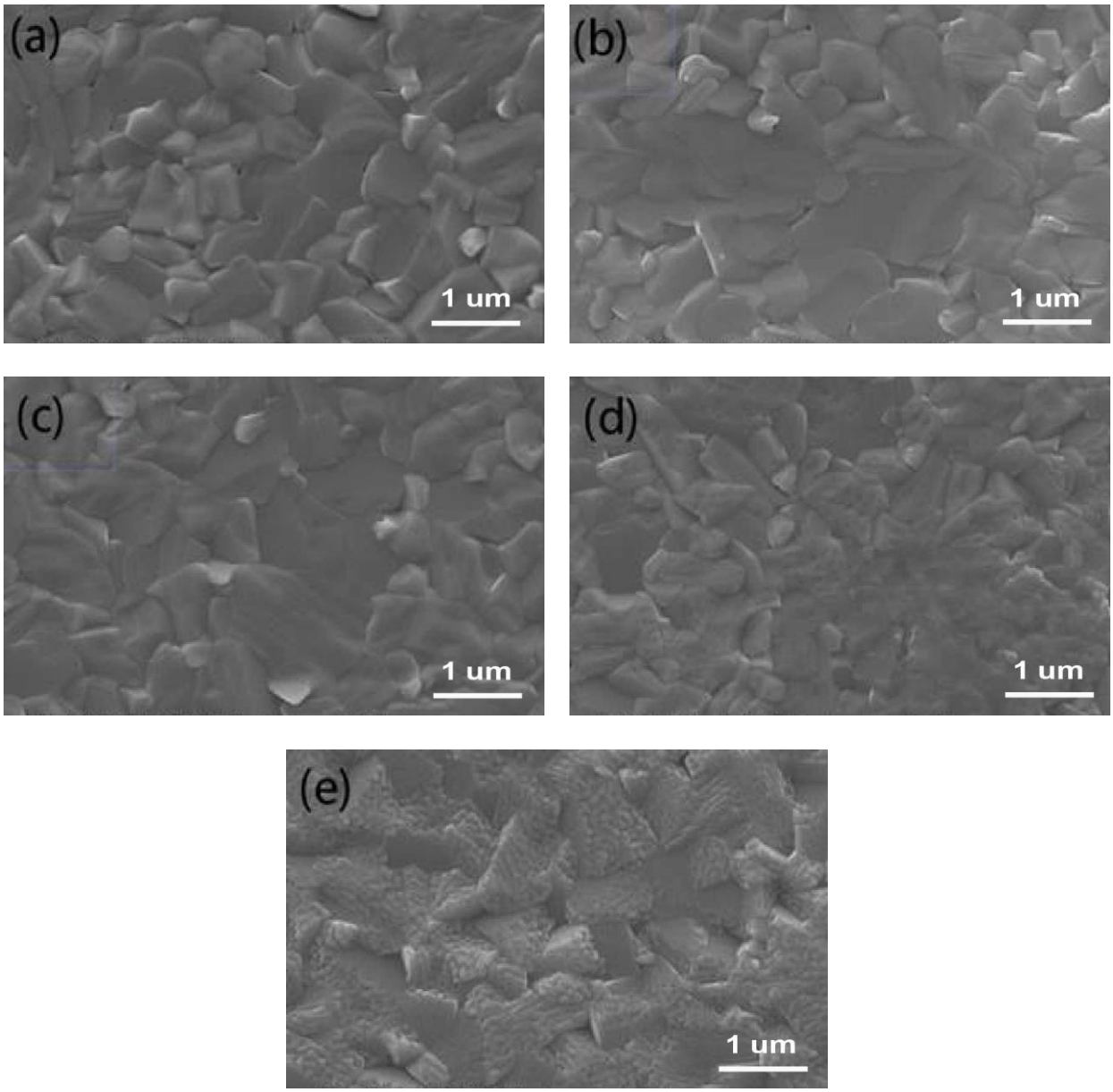

Fig. 6. Surface SEM images of SnSe thin films with different doping amount of Zn((a) 0% Zn doping, (b) 0.285% Zn doping, (c) 0.501% Zn doping, (d) 0.823% Zn doping, (e) 0.978% Zn doping)

The shape of the grains changes with increasing the doping amount of Zn, which indicates that Zn has been successfully doped in SnSe thin films, consistent with the results from the XRD measurements as Fig. 5(a) shows. It can be easily seen that the grain size of the SnSe thin films with 0.285% Zn-doped and 0.501% Zn-doped is larger than other SnSe thin films in this work, which indicates an enhanced grain growth and better crystallinity with a little doping amount of Zn. Usually, it is important to acquire the absorber films with better crystallinity or large grain size for high energy conversion efficiency since smaller grains will lead to recombination, which lead to the decrease of open circuit voltage and a reduction in current [38].

3.4. Electrical properties

Fig. 7 shows the electrical properties of the undoped and Zn-doped SnSe thin films measured by Hall Effect measurement system using Van der Pauw method and four-point probes at room temperature. All films are p-type semiconductors. As is shown in Fig. 7, SnSe thin film with 0.285% Zn-doped indicates the highest electron

mobility (32.69 $cm^2V^{-1}s^{-1}$) and relative lower resistivity (1.32 Ωcm), which results from the larger grain size and better crystallinity. And high carrier mobility is required for improving the solar cell conversion efficiency. Although the electron mobility of SnSe thin film with 0.501% Zn-doped is higher than others despite SnSe thin film with 0.285% doping amount of Zn, the relative higher resistivity (2.98 Ωcm) may limit the power conversion efficiency. Hence, the SnSe thin film (obtained with 0.285% Zn-doped in this work) with higher carrier mobility and relative lower resistivity may be more appropriated for application in photovoltaic device.

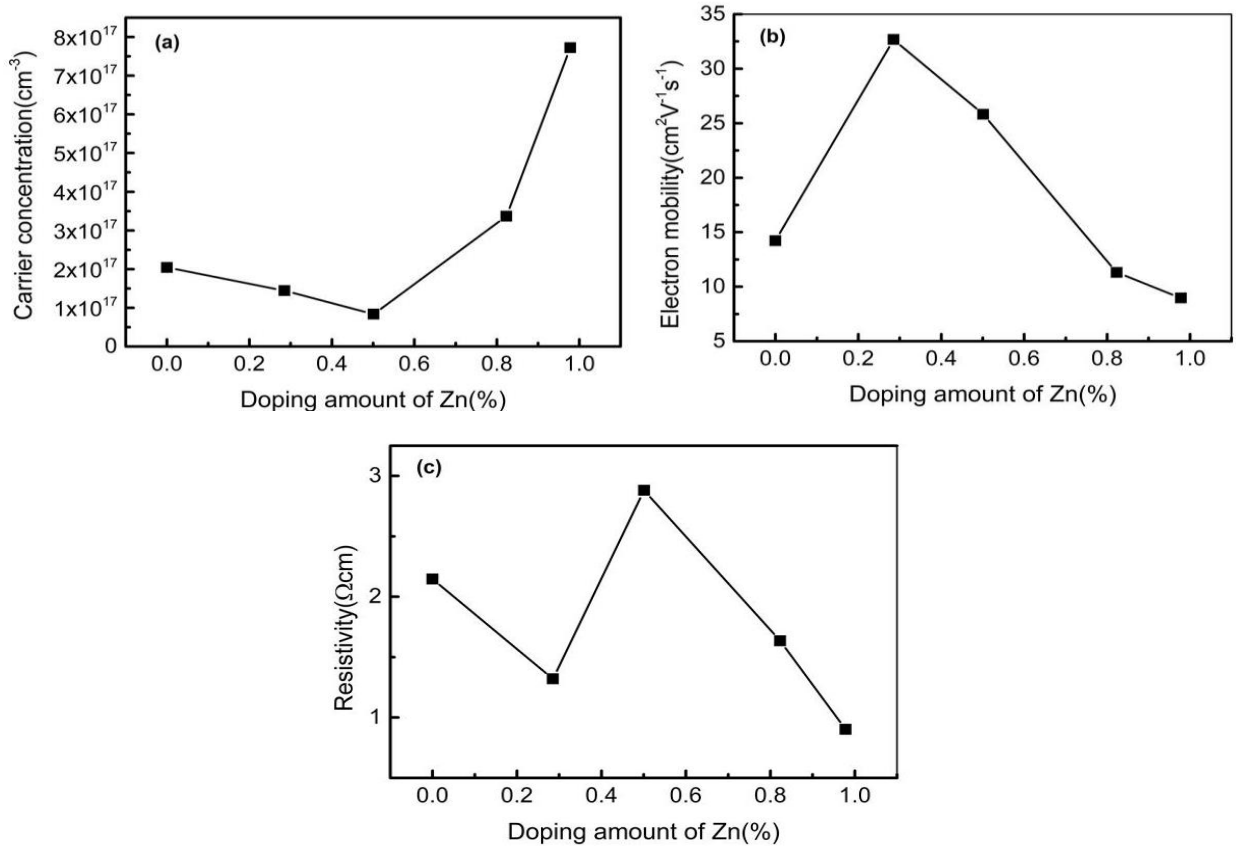

Fig. 7. (a) Carrier concentration, (b) Electron mobility and (c) Resistivity of SnSe thin films with different doping amount of Zn

3.5. J-V curves

Fig. 8 shows the J-V curves measured for undoped and Zn-doped SnSe thin film solar cells under AM1.5 1-Sun irradiation condition at room temperature. The doping amount of Zn plays an important role in power conversion efficiency of the SnSe thin film solar cell as the influences on electrical, optical and structural properties. Table 2 shows the device parameters of the fabricated solar cells. The devices fabricated with absorbers were deposited and show the best efficiency (η) of 0.55% with an open circuit voltage (V_{oc}) of 116 mV, short-circuit current density (J_{sc}) of 14.85 mA/cm^2, and fill factor (FF) of 31.84% with the 0.285% doping amount of Zn. It can be seen that the short-circuit current density (J_{sc}), open-circuit voltage (V_{oc}) and fill factor (FF) were improved obviously for solar cell with 0.285% doping amount of Zn compared to undoped SnSe thin film solar cell, which resulted in the final power conversion efficiency (η) from 0.19% to 0.55% as the Table 2 shows. The improvements for the sample with 0.285% doping amount of Zn was mainly attributed to the better crystallinity, larger grain size, higher carrier mobility and lower resistivity obtained in this work.

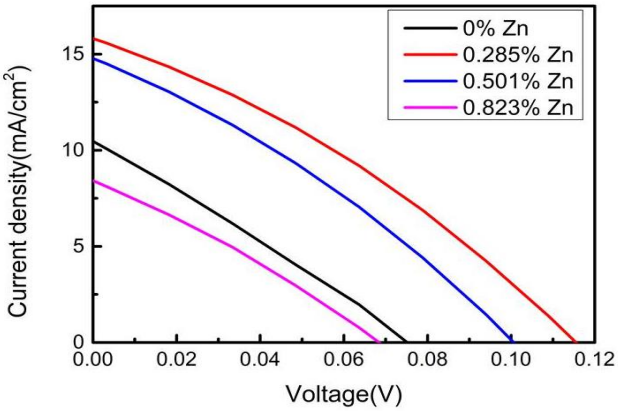

Fig. 8. The J-V characteristics of SnSe thin film solar cells with different doping amount of Zn (color online)

Table 2. The device parameters of the fabricated solar cells

Doping amount of Zn (%)	V_{oc} (mV)	J_{sc} (mA/cm^2)	FF (%)	η (%)
0	75	9.76	26.77	0.19
0.285	116	14.85	31.84	0.55
0.501	101	13.79	30.89	0.42
0.823	68	7.85	28.89	0.15

4. Conclusions

The structure, optical properties, morphology and electrical properties of the SnSe thin films with different doping amount of Zn were investigated. The crystallinity and grain size of SnSe thin films are different by changing the doping amount of Zn. Better crystallinity and larger grain size were obtained of SnSe thin films with 0.285% Zn-doped. The direct band gap of SnSe thin films between 0.9 and 1.1 eV and the value of indirect band gap of SnSe thin films between 0.86 and 0.98 eV were obtained. All the films exhibited p-type conductivity and a lower resistivity of 1.32 Ωcm and maximum electron mobility of 32.69 $cm^2V^{-1}s^{-1}$ was obtained with 0.285% Zn-doped. All films have characteristics of preferential (111) planar orientation. Finally, the manufactured SnSe solar cell exhibits a high power conversion efficiency of 0.55%.

Acknowledgements

This work was financed by Major State Basic Research Development Program of China (Grant No. 2013CB922300).

References

[1] Y. Guo, J. Tao, J. Jiang, J. Zhang, J. Yang, S. Chen, J. Chu, Sol. Energy Mater. Sol. Cells **188**, 66 (2018).

[2] Y. Guo, J. Jiang, S. Zuo, F. Shi, J. Tao, Z. Hu, J. Chu, Sol. Energy Mater. Sol. Cells **178**, 186 (2018).

[3] F. Zhao, Y. Guo, X. Wang, J. Tao, J. Jiang, Z. Hu, J. Chu, Sol. Energy **191**, 263 (2019).

[4] Y. Gelbstein, B. Dado, O. Ben-Yehuda, Y. Sadia, Z. Dashevsky, M. P. Dariel, J. Electron. Mater. **39**, 2049 (2010).

[5] M. A. Green, E. D. Dunlop, D. H. Levi, J. Hohl-Ebinger, M. Yoshita, A. W. Ho-Baillie, Prog. Photovolt: Res. Appl. **7**, 565 (2019).

[6] N. G. Dhere, Sol. Energy Mater. Sol. Cells **95**, 277 (2011).

[7] M. A. Franzman, C. W. Schlenker, M. E. Thompson, R. L. Brutchey, J. Am. Chem. Soc. **132**, 4060 (2010).

[8] N. R. Mathews, Sol. Energy **86**, 1010 (2012).

[9] F. K. Butt, M. Mirza, C. Cao, F. Idrees, M. Tahir, M. Safdar, Z. Ali, M. Tanveer, I. Aslam, Cryst. Eng. Comm. **16**, 3470 (2014).

[10] J. Ning, G. Xiao, T. Jiang, L. Wang, Q. Dai, B. Zou, G. Zou, Cryst. Eng. Comm. **13**, 4161 (2011).

[11] E. Barrios-Salgado, M. T. S. Nair, P. K. Nair, ECS J. Solid State Sci. Technol. **3**, Q169 (2014).

[12] V. R. M. Reddy, S. Gedi, B. Pejjai, C. Park, J. Mater. Sci. Mater. Electron. **27**, 5491 (2016).

[13] Z. Li, Y. Guo, F. Zhao, C. Nie, H. Li, J. Shi, S. Zuo, RSC Advances **10**, 16749 (2020).

[14] C. Tang, Q. Li, C. Zhang, C. He, J. Li, T. Ouyang, J. Zhong, J. Phys. D: Appl. Phys. **51**, 245004 (2018).

[15] D. D. Cuong, S. H. Rhim, J. Lee, S. Hong, AIP Adv. **5**, 117147 (2015).

[16] A. Ghosh, M. S. Gusmo, P. Chaudhuri, S. M. Souza, C. Mota, D. M. Trichês, H. O. Frota, Comput. Condens. Matter. **9**, 77 (2016).
[17] Z. Y. Hu, K. Y. Li, Y. Lu, Y. Huang, X. H. Shao, Nanoscale **9**, 16093 (2017).
[18] Q. Wang, W. Yu, X. Fu, C. Qiao, C. Xia, Y. Jia, Phys. Chem. Chem. Phys. **18**, 8158 (2016).
[19] X. L. Wang, W. Li, T. X. Wang, X. Q. Dai, Phys. E **75**, 106 (2016).
[20] Y. Wu, W. Xia, W. Gao, W. Ren, P. Zhang, Phys. Rev. Appl. **8**, 034007 (2017).
[21] L. C. Zhang, G. Qin, W. Z. Fang, H. J. Cui, Q. R. Zheng, Q. B. Yan, G. Su, Sci. Rep. **6**, 1 (2016).
[22] M. Zhou, X. Chen, M. Li, A. Du, J. Mater. Chem. C **5**, 1247 (2017).
[23] Z. Zainal, N. Saravanan, K. Anuar, M. Z. Hussein, W. M. M. Yunus, Mater. Sci. Eng. B **107**, 181 (2004).
[24] M. Bicer, I. Sisman, Appl. Surf. Sci. **257**, 2944 (2011).
[25] F. K. Butt, C. Cao, W. S. Khan, Z. Ali, R. Ahmed, F. Idrees, T. Mahmood, Mater. Chem. Phys. **137**, 565 (2012).
[26] N. D. Boscher, C. J. Carmalt, R. G. Palgrave, I. P. Parkin, Thin Solid Films **516**, 4750 (2008).
[27] F. Jamali-Sheini, F. Niknia, M. Cheraghizade, R. Yousefi, M. R. Mahmoudian, Chem. Electro. Chem. **4**, 1478 (2017).
[28] M. Cheraghizade, F. Jamali-Sheini, Appl. Phys. A **123**, 390 (2017).
[29] F. Jamali-Sheini, M. Cheraghizade, F. Niknia, R. Yousefi, MRS Commun. **6**, 421 (2016).
[30] M. A. Baghchesara, R. Yousefifi, M. Cheraghizade, F. Jamali-Sheini, A. Saaedi, Vacuum **123**, 131 (2016).
[31] J. Ahmad, H. Minami, S. Alam, J. Yu, Y. Arai, H. Uwe, Chinese Physics Letters, **25** 4421 (2008).
[32] P.K. Ghosh, S. F. Ahmed, S. Jana, K. K. Chattopadhyay, Opt. Mater. **29**, 1584 (2007).
[33] J. P. Singh, J. Mater. Sci. Mater. Electron. **2**, 105 (1991).
[34] B. Pejova, I. Grozdanov, Thin Solid Films **515**, 5203 (2007).
[35] D. T. Quan, Phys. Stat. Sol. A **86**, 421 (1984).
[36] R. Teghil, A. Santagata, V. Marotta, S. Orlando, G. Pizzella, A. Giardini-Guidoni, A. Mele, Appl. Surf. Sci. **90**, 505 (1995).
[37] G. Jeong, J. Kim, O. Gunawan, S. R. Pae, S. H. Kim, J. Y. Song, B. Shin, J. Alloys Compd. **722**, 474 (2017).
[38] J. W. Li, D. B. Mitzi, V. B. Shenoy, ACS Nano **5**, 8613 (2011).

*Corresponding author: fzhaobs@126.com